Antiferromagnetic triangular Blume-Capel model with hard-core exclusions

A. Ibenskas, M. Šimėnas, and E. E. Tornau*

Semiconductor Physics Institute, Center for Physical Sciences and Technology, Goštauto 11, LT-01108 Vilnius, Lithuania

(Received 6 February 2014; revised manuscript received 7 May 2014; published 29 May 2014)

Using Monte Carlo simulation, we analyze phase transitions of two antiferromagnetic (AFM) triangular Blume-Capel (BC) models with AFM interactions between third-nearest neighbors. One model has hard-core exclusions between the nearest-neighbor (1NN) particles (3NN1 model) and the other has them between the nearest-neighbor and next-nearest-neighbor particles (3NN12 model). Finite-size scaling analysis reveals that in these models, the transition from the paramagnetic to long-range order (LRO) AFM phase is either of the first order or goes through an intermediate phase which might be attributed to the Berezinskii-Kosterlitz-Thouless (BKT) type. The properties of the low-temperature phase transition to the AFM phase of the 1NN, 3NN1, and 3NN12 models are found to be very similar for almost all values of a normalized single-ion anisotropy parameter, $0 < \delta < 1.5$. Higher temperature behavior of the 3NN12 and 3NN1 models is rather different from that of the 1NN model. Three phase transitions are observed for the 3NN12 model: from the paramagnetic phase to the phase with domains of the LRO AFM phase at T_c, from this structure to the diluted frustrated BKT-type phase at T_2, and from the frustrated phase to the AFM LRO phase at T_1. For the 3NN12 model, $T_c > T_2 > T_1$ at $0 < \delta < 1.15$ (range I), $T_c \approx T_2 > T_1$ at $1.15 < \delta < 1.3$ (range II), and $T_c = T_2 = T_1$ at $1.3 < \delta < 1.5$ (range III). For the 3NN1 model, $T_c \approx T_2 > T_1$ at $0 < \delta < 1.2$ (range II) and $T_c = T_2 = T_1$ at $1.2 < \delta < 1.5$ (range III). There is only one first-order phase transition in range III. The transition at T_c is of the first order in range II and either of a weak first order or a second order in range I.

DOI: 10.1103/PhysRevE.89.052144 PACS number(s): 64.60.Ht

I. INTRODUCTION

In recent years, the self-assembly of large triangular molecules has attracted a great deal of attention (see, e.g., Refs. [1,2]). Trimesic acid (TMA) [3–8], BTB [9,10], melamine [11–13], and some other molecules [14–16] create patterns of different complexity on the solid-liquid interface or in ultravacuum conditions on graphite and metal surfaces. The assemblies of such molecules might be different, but the so-called honeycomb phase is the dominating low-temperature pattern.

The statistical models of phase transitions are used to characterize the ordering of such molecules. The honeycomb phase is represented by the low-temperature long-range order (LRO) phase on a tripartite lattice with the sites of each sublattice occupied by occupation variables $+1$, -1, and 0, respectively. For example, the "tip-to-tip" ordering of triangular TMA molecules might be described [17] by the antiferromagnetic (AFM) nearest-neighbor (1NN) three-state Bell-Lavis model, which was originally created [18,19] to describe the ordering of lattice fluids. It is similar to better known triangular AFM lattice models: the Blume-Capel (BC) model [20–23] with some neglected interactions, the Blume-Emery-Griffiths model [24] with anisotropic term [25,26], and the diluted triangular AFM Ising (TAFI) model [27]. The "side-to-side" ordering of melamine molecules [13] into the honeycomb phase represents the ordering typical for a triangular AFM BC model.

Hard-core exclusions (infinite repulsive interactions) are introduced to account for a finite size of large molecules. To describe the assembly of TMA molecules into a series of flower phases, a model [28] with rescaled initial lattice was proposed. In this model, the molecular interactions, which mimic the H bonds, act between the molecules being on third-nearest-neighbor (3NN) sites, and the exclusion is introduced at 1NN distance.

At least two important questions arise when triangular AFM and other lattice models are used to describe the molecular ordering (see, e.g., [12,13,29–32]): to what extent might the standard models be rescaled and what effect does the exclusion bring in comparison with classical (i.e., usually 1NN) statistical models? Intuitively, it is clear that the rescaling to the nNN models (with $n > 1$) changes the entropy of the system, repressing the ordered phases and decreasing the phase transition temperature, since there are more sites for molecular diffusion. On the other hand, the exclusion decreases the number of sites for diffusion, and promotion of the ordered phases increases the transition temperature.

Here we try to answer these questions using a triangular AFM BC model with exclusions. This model is closely related to the TAFI model, which was extensively studied [27] due to its frustrated phase and large entropy at $T = 0$. The TAFI model with magnetic field (chemical potential) gives rise to the ordered three-sublattice structure, denoted as $\sqrt{3} \times \sqrt{3}$, in which magnetizations (densities) of two sublattices are equal, but different from that of the third [33]. When diluted by nonfixed vacancies, which evolve together with the spins (the so-called annealed vacancies), the TAFI model also allows for the three-sublattice LRO structure. Simple substitution of the occupation variables [34] transforms the diluted TAFI model in a field into the Ising spin-1 or BC model [20]. The TAFI model can also be mapped into a six-state AFM clock model [35]. As shown by Cardy [36], the six-state clock model can exhibit either a first-order transition, two Berezinskii-Kosterlitz-Thouless (BKT)-type transitions, or successive Ising, three-state Potts, or Ashkin-Teller-like transitions. With decrease of temperature, the six-state AFM clock model on the triangular lattice gives rise to two very close phase transitions, which are attributed to the Ising (chiral) and BKT type, respectively [37,38].

*et@et.pfi.lt

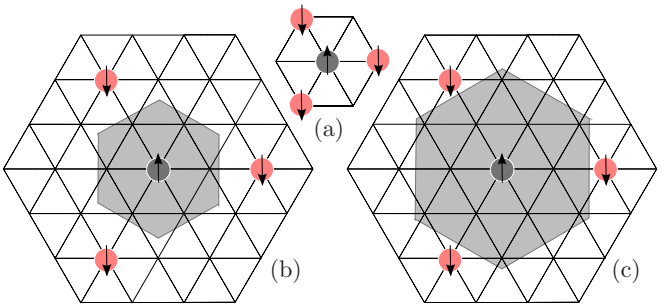

FIG. 1. (Color online) Particle (spin) arrangement in the LRO AFM phase on triangular lattice for (a) 1NN, (b) 3NN1, and (c) 3NN12 models. Gray regions schematically mark the limits of exclusion (infinite repulsion) for the central spin.

The earliest studies [21] of the triangular AFM BC model, performed by renormalization group methods, demonstrated that this model exhibits the AFM LRO phase, which has the sites of its three sublattices occupied by variables 1, −1, and 0, respectively. This phase occurs when the ratio of a single-ion anisotropy parameter, normalized to antiferromagnetic coupling, $\delta = \Delta/|J|$, is between 0 and 3/2. If $\delta > 3/2$, the gas (disordered) phase prevails. At $\delta < 0$, the frustrated phase, typical for the TAFI model, exists. The phase transitions to the LRO phase were shown [21] to be of the second order for all $\delta > 0$, except those first-order transitions which occur close to the boundary of the LRO phase, $\delta \to 3/2$. It should be noted that by treating the model spin variables as particle variables and using the lattice-gas rather than the magnetic formalism, the single-ion anisotropy parameter δ might be interpreted as a chemical potential. In this case, the decrease of δ is associated with an increase of particle concentration at the expense of vacancies and transition from the three-state AFM BC model to the two-state TAFI model (no vacancies) at $\delta = 0$.

A recent Monte Carlo (MC) study [39] of phase transitions for the AFM BC model revealed that the phase transition from the paramagnetic to the AFM LRO phase is mediated by the BKT-type phase in a whole interval of $\delta > 0$, except for $\delta \gtrsim 1.47$, where the first-order phase transition between the paramagnetic and LRO AFM phases was found.

In this paper, we study the AFM BC model with exclusions. The problem is solved by assuming the AFM interaction of spins residing on the 3NN sites. Two models with hard-core exclusions are considered: the 3NN model with exclusions at the 1NN sites (3NN1) and the 3NN model with 1NN and 2NN exclusions (3NN12) (see Fig. 1). It should be noted that the 3NN AFM BC model without exclusions is not studied here because it yields an entirely different type of LRO AFM phase as its ground state structure.

The obtained results for the 3NN1 and 3NN12 models are compared with the results of the 1NN model. We study how the exclusions affect the type of phase transition, the critical line of the BKT points, and the phase diagram. The phase diagrams of all three models are presented in the last section. In both 3NN models with exclusions, we obtain the same phase transitions to the BKT-type phase which were obtained in the 1NN model. However, the similarity extends only to low temperature and those values of a single-ion anisotropy parameter which are not close to the gas phase limit. At higher temperature and close to this limit, the properties are different. The exclusions decrease the high-temperature point of the BKT-type phase transition and might stimulate the occurrence of a transition from the paramagnetic phase to the structure with domains of the LRO AFM phase.

II. MODEL AND DETAILS OF SIMULATION

The model Hamiltonian has the form

$$\mathcal{H} = -J \sum_{i,j} s_i s_j + \Delta \sum_i s_i^2, \tag{1}$$

where $s_i = \pm 1, 0$ is the spin variable on the triangular lattice site i, J is the antiferromagnetic ($J < 0$) interaction parameter acting between the particles at 3NN sites, and Δ is a single-ion anisotropy parameter. Here we regard the introduced variables as describing the magnetic particles in the diluted lattice-gas model rather than the spin projections. Therefore, in (1), we write Δ with plus sign and treat this parameter as a chemical potential, i.e., the total concentration of ± 1 particles increases (decreases) with decrease (increase) of Δ. In the 3NN12 model, the interactions between particles separated by 1NN and 2NN distances are forbidden by taking infinite repulsion of particles at these sites. In the 3NN1 model, the interactions between particles in the 1NN sites are forbidden in the same way. Further, the temperature and single-ion anisotropy parameter are both normalized to $|J|$: $k_B T/|J|$ and $\delta = \Delta/|J|$.

Since cluster algorithms for frustrated systems are known to be ineffective [40], we performed the simulation of phase transition properties using the local update (single-flip) Metropolis algorithm and Glauber dynamics. In the beginning, the sites of a triangular lattice were randomly populated by particles in states +1, 1, and 0, and the initial energy E_i of a randomly chosen molecule was calculated. Then the initial state of that molecule was changed (with equal probability) to one of two remaining states, and the final energy E_f was calculated. The new state was accepted if the energy decreased after the change of state, or accepted with the probability $\sim \exp[-(E_f - E_i)/k_B T]$ if the energy increased. The calculations were performed with fixed δ (chemical potential), while the concentration of particles in the nonzero state was allowed to vary.

For thermal averaging MC calculations and finite-size scaling (FSS) of both 3NN models with exclusions, we used the triangular lattices of sizes $L \times L$, with L from 96 up to 288. For calculations of the 1NN model, which we performed to compare the results, the lattice sizes $L = 48$, 72, 96, 120 were used [for the 1NN model, J in (1) is acting between the particles on the 1NN sites]. We used periodic boundary conditions and $(0.2 - 1) \times 10^6$ MC steps (MCS) for thermalization. We estimated the thermalization period by observing the time evolution of the order parameter and energy. The tests were performed at different temperatures. Before gathering statistics for thermal averaging, we also made additional checks at multiple temperatures near phase transition points, in order to verify that the sample had entered an equilibrium state. The thermalization time did not exceed 10^5 MCS for small lattices and 10^6 MCS for large lattices and close to first-order phase transitions.

Further, we collected averages of 10^7 MCS for the 3NN models and 10^6–10^7 MCS for the 1NN model and smaller lattices of the 3NN models. Our simulations were performed starting from higher temperature (paramagnetic phase) and using random initial particle configuration. Then the temperature was gradually decreased in small steps with simulations at the new temperature starting from the final configuration of the previous temperature.

To estimate statistical errors, we used the data from $n \approx 5$ independent simulation runs, all starting from different initial states. The observation x_i of each run was used to obtain a mean value $\bar{x}$ at that particular temperature. The error bar of $\bar{x}$ is given by $\sigma = s/\sqrt{n-1}$ and $s^2 = \frac{1}{n}\sum_{i=1}^{n}(x_i - \bar{x})^2$.

We also performed the analysis of the autocorrelation time of energy at T_c at $\delta = 0.7$ for both 3NN models. The integrated autocorrelation time for the 3NN12 model ranged from $\tau \sim 10^3$ MCS for $L = 120$ to $\tau \sim 10^5$ MCS for $L = 399$. For the 3NN1 model, this time is around one to two orders of magnitude higher.

The studied system was often characterized by abruptness of thermodynamic parameters and first-order phase transitions. Therefore, we performed energy histogram calculations using single-histogram reweighting techniques [41]. For these calculations, we used lattice sizes $L = 120$–270. In a few cases, we employed very large lattice sizes, $L = 360$ and 399. We omitted the first 10^6 MCS and used 2×10^7 MCS to gain reliable statistics.

Our simulations of thermodynamic parameters (energy derivatives) often proceeded as follows: the phase transition point was located by thermal averaging and then recalculated at the phase transition point using the reweighting scheme. The results were considered reliable if the data obtained by both methods matched.

For studies of phase transitions, we used the AFM order parameter. It should be noted that the low-temperature AFM phase of the 1NN model is stabilized when each sublattice of the tripartite lattice is occupied by $+1$, -1, and 0 variables, respectively. The distance between so-occupied sites is one lattice constant of a triangular lattice, a. The particle concentration (coverage of sites occupied by the ± 1 particles) is $c = \sum_i s_i^2/L^2$. The stoichiometric concentration in the 1NN model is $c_s = 2/3$. The low-temperature AFM phase of both 3NN models has 12 sublattices, only two of which are occupied by the $+1$ and -1 particles, respectively, and all other sublattices are empty. Therefore, the distance between $+1$ and -1 particles is $2a$ and $c_s = 1/6$ in the AFM phase of both 3NN models. As an order parameter, we use the staggered magnetization, a slightly revised version of the one suggested for the 1NN model [39]. It is the average difference of maximally and minimally occupied sublattices. For the 3NN model, we had to account for the occupancy of 12 sublattices, and therefore the staggered magnetization has the form

$$m_s = \langle M_s \rangle / L^2 = 6 \left\langle \max\left(\sum_{i1 \in \mathrm{sub1}} s_{i1}, \sum_{i2 \in \mathrm{sub2}} s_{i2}, \ldots, \sum_{i12 \in \mathrm{sub12}} s_{i12} \right) - \min\left(\sum_{i1 \in \mathrm{sub1}} s_i, \sum_{i2 \in \mathrm{sub2}} s_{i2}, \ldots, \sum_{i12 \in \mathrm{sub12}} s_{i12} \right) \right\rangle \Big/ L^2. \quad (2)$$

Here, $i1, \ldots, i12$ denote sites belonging to each sublattice, and the factor 6 is needed to compensate for the stoichiometric concentration of the AFM phase in the 3NN models. We also calculate the temperature dependences of the specific heat, $C_v = (\langle \mathcal{H}^2 \rangle - \langle \mathcal{H} \rangle^2)/L^2 k_B T^2$, susceptibility $\chi = (\langle M_s^2 \rangle - \langle M_s \rangle^2)/L^2 k_B T$, logarithmic derivatives of $\langle M_s \rangle$ and $\langle M_s^2 \rangle$,

$$D_{1s} = \frac{\partial \ln \langle M_s \rangle}{\partial \beta} = \frac{\langle M_s \mathcal{H} \rangle}{M_s} - \langle \mathcal{H} \rangle,$$
$$D_{2s} = \frac{\partial \ln \langle M_s^2 \rangle}{\partial \beta} = \frac{\langle M_s^2 \mathcal{H} \rangle}{M_s^2} - \langle \mathcal{H} \rangle, \quad (3)$$

and Binder order parameter and energy cumulants, $U_B^m = 1 - \langle M_s^4 \rangle / 3 \langle M_s^2 \rangle^2$ and $U_B^E = 1 - \langle \mathcal{H}^4 \rangle / 3 \langle \mathcal{H}^2 \rangle^2$, respectively. The functions D_{1s} and D_{2s} were introduced in Ref. [42]. They were shown [39] to be useful for a finite-size scaling of the 1NN AFM BC model. At the second-order phase transition point T_c, the maximum of specific heat and susceptibility scale as $C_v \sim L^{\alpha/\nu}$ and $\chi \sim L^{\gamma/\nu}$, respectively, while the minimum of D_{1s} and D_{2s} scale as $\sim L^{1/\nu}$. Here, α, β, and ν are critical exponents of specific heat, susceptibility, and correlation length, respectively. At the first-order phase transition at T_c, the extrema of all these functions scale as $\sim L^d$ [43], where d is the dimensionality of the system.

In a following section, we present the values of critical exponent ratios α/ν and $1/\nu$ at the phase transition point from the paramagnetic phase, T_c. The ratio α/ν is obtained either by the combined thermal averaging and reweighted histogram calculation of the specific heat maximum at T_c or by scaling these values close to T_c and using the formula $C_v - C_0 \sim L^{\alpha/\nu} f(tL^{1/\nu})$ (here, $t = |T_c - T|/T_c$ and the background is assumed to be $C_0 = 0$). The latter formula also gives the value of $1/\nu$, which we alternatively obtain as the average of scaling of parameters D_{1s} and D_{2s}.

In a case of a BKT-type phase transition, the correlation length diverges as $\xi = \xi_0 \exp\{a[(T_{\mathrm{BKT}} - T)/T_{\mathrm{BKT}}]^{-1/2}\}$ and the spin-correlation function decays as $\langle s_i s_j \rangle \sim r_{ij}^{-\eta}$, where η is the critical exponent of the correlation function [44]. The order parameter at the BKT-type phase transition point scales as $m_s(L) \sim L^{-\eta/2}$. The exponent η might also be obtained from a part of susceptibility $\chi' = \langle M_s^2 \rangle / L^2 k_B T \sim L^{2-\eta}$ [45]. To obtain accurate values of the BKT-type phase transitions of the AFM BC 1NN model at T_1 and T_2, the FSS of parameters m_s and χ' was performed [39]. The following relations were used:

$$m_s L^b = f_1 \left\{ L^{-1} \exp\left[a \left(\frac{T_1 - T}{T_1} \right)^{-1/2} \right] \right\}, \quad T < T_1,$$
$$\chi' L^c = f_2 \left\{ L^{-1} \exp\left[a \left(\frac{T - T_2}{T_2} \right)^{-1/2} \right] \right\}, \quad T > T_2, \quad (4)$$

where $b = \eta/2$ and $c = 2 - \eta$, and T_1 and T_2 are the lower-temperature AFM LRO phase—frustrated (BKT-type) phase and higher-temperature frustrated phase—paramagnetic phase transition temperatures, respectively.

III. RESULTS OF SIMULATION

Here the phase transitions of both 3NN models are demonstrated and classified at $0 < \delta < 1.5$. We found three ranges of phase transitions for the 3NN12 model. In range I ($0 < \delta < 1.15$), there are three phase transitions: two of them, at T_1 and T_2, confine the BKT-type phase, and the third is a high-temperature phase transition at T_c. In range II ($1.15 < \delta < 1.3$), the BKT-type phase remains, but $T_2 \approx T_c$. This range is found also for the 3NN1 model at $0 < \delta < 1.2$.

In the remaining range III, there is just one first-order phase transition at $T_1 = T_2 = T_c$. This range is found for both 3NN12 and 3NN1 models and it also exists in the 1NN model at $\delta > 1.47$. In between 0 and 1.47, the 1NN model demonstrates just the two transitions bounding the BKT-type phase [39].

A. 3NN12 model at $\delta = 0.7$ (range I)

The temperature dependence of staggered magnetization [Fig. 2(a)] demonstrates that there are three phase transitions at $\delta = 0.7$. In addition to two transitions at T_1 and T_2 [which correspond to two peaks of susceptibility in Fig. 2(b)], the high-temperature phase transition at T_c is nicely visible as a twist of $m_s(T)$ dependence at very low values of $m_s < 0.05$. In the temperature dependence of susceptibility, the T_c point might be seen as a small higher-temperature shoulder of the peak at T_2. However, the transition at T_c is manifested by the main high-temperature peak of the $C_v(T)$ dependence [Figs. 2(b) and 2(d))], where the transition at T_2 is its hardly discernible lower-temperature satellite [Fig. 2(c)]. The transition at T_1 is very weakly L dependent [Fig. 2(e)].

All three transitions are best manifested as minima [see Fig. 3(a)] in temperature dependences of parameters D_{1s} and D_{2s} (3), which combine the contribution of energy and order parameter. In Figs. 3(b) and 3(c), where the Binder cumulants of energy and magnetization are presented, the transition at T_1 is seen as a smooth continuous step and the transition at T_c is seen as a deep minimum. The transition at T_2 is not seen in U_B^E, but is clearly seen in U_B^m in between the transitions at T_1 and T_c.

Visually, the $m_s(T)$ dependence between the transition points at T_1 and T_2 is similar to that obtained for the 1NN model. An analysis of log-log plots of magnetization vs L [Fig. 4(a)] corroborates the finding of the 1NN model that the transitions at T_1 and T_2 belong to the BKT-type phase transitions. This is seen from the temperature dependence of the critical exponent of the correlation function, η [Fig. 4(b)], which for the BKT-type transitions should correspond to the doubled slope of lines in Fig. 4(a). In the temperature range between 0.35 and 0.55, the parameter η clearly demonstrates a plateau. The interval of η values in the plateau roughly coincides with classical predictions for the critical line of the BKT-type phase transitions [46]. We performed the FSS analysis using formula (4) to obtain more accurate values of transition temperatures T_1 and T_2 as well as η. The results are shown in Figs. 5(a) and 5(b). The best fit was obtained for the values $k_B T_1/|J| = 0.35 \pm 0.01$, $\eta(T_1) = 0.12 \pm 0.02$ and $k_B T_2/|J| = 0.55 \pm 0.01$, $\eta(T_2) = 0.29 \pm 0.02$. Here, as in the 1NN model, the obtained value of T_1 is a bit higher than that at the peak of C_v and very similar to that at the peak of χ, while T_2 lies lower than that obtained at the peak of χ.

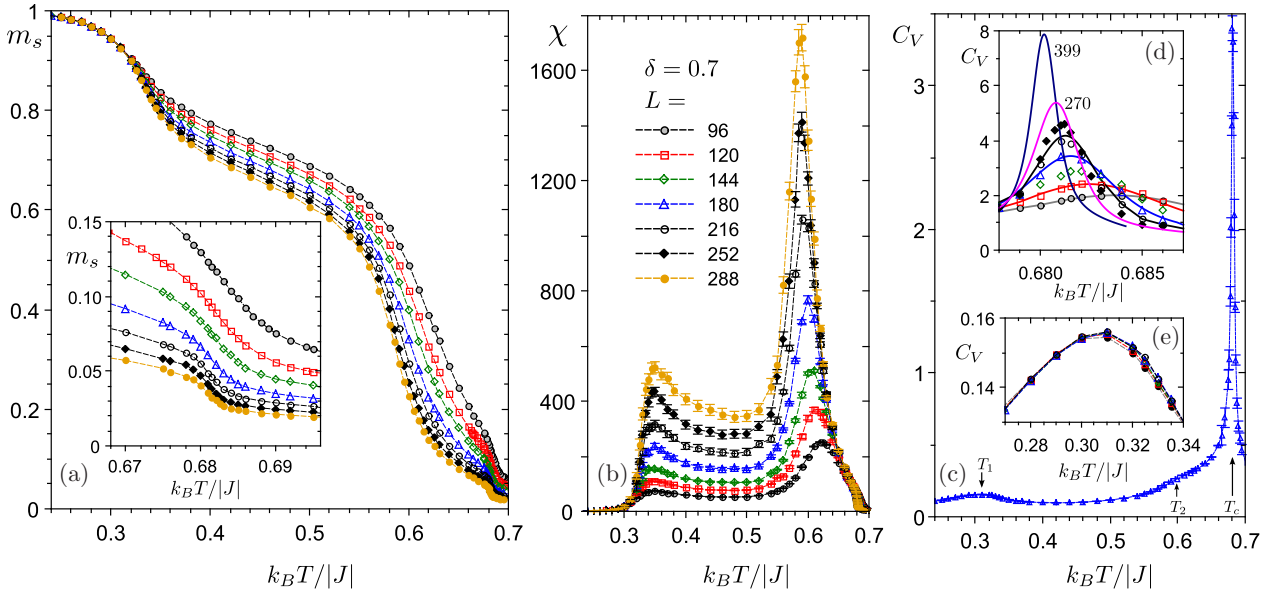

FIG. 2. (Color online) Temperature dependence of (a) staggered magnetization and (b) susceptibility of the 3NN12 model at $\delta = 0.7$ for different values of L. Inset in (a): Magnified behavior of $m_s(T)$ at T_c. Errors in (a) do not exceed symbol size. Dashed lines in (a) and (b) are guides to the eye. (c) Temperature dependence of specific heat of the 3NN12 model at $\delta = 0.7$ and $L = 180$. Insets in (c): $C_v(T)$ dependence around (d) T_c and (e) T_1 for different values of L. The symbols and solid lines in (d) denote the results of thermal averaging and reweighting, respectively.

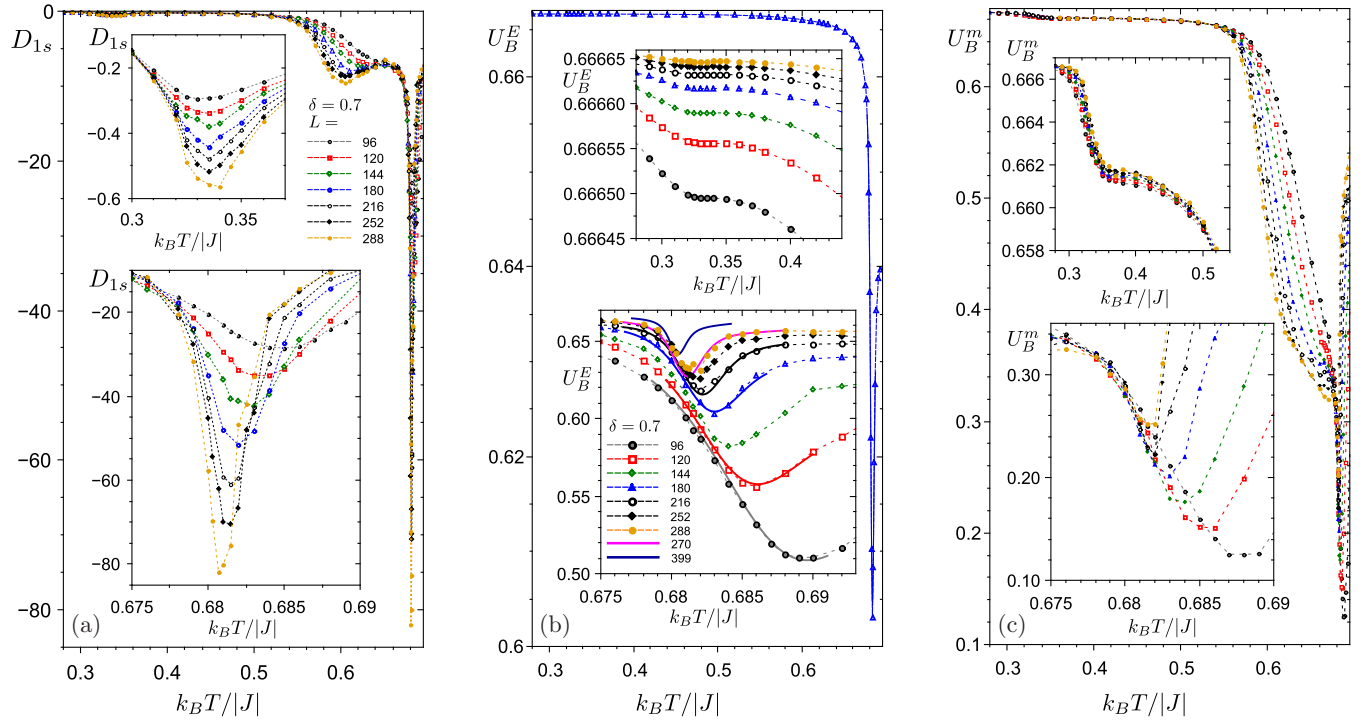

FIG. 3. (Color online) Temperature dependence of (a) parameter D_{1s} and Binder cumulants (b) U_B^E and (c) U_B^m of the 3NN12 model at $\delta = 0.7$ and different values of L. Magnified dependences close to transitions at T_1 and T_c are shown in the upper and lower insets, respectively. Symbols correspond to thermal averaging results; dashed lines are guides to the eye. In lower inset of (b), the results of histogram reweighting close to T_c are shown by solid lines.

Note that we expected some error in the determination of the T_2 point, since in the 3NN12 model, differently from the 1NN model, the transition at T_2 is not from the paramagnetic phase. Still, as might be seen from Fig. 5(b), the scaling is quite satisfactory.

The η interval of the BKT points is rather close to the one obtained in similar models: the 1NN model (0.12–0.29) [39], the planar rotator model with sixfold symmetry breaking fields (1/9–1/4) [46], six-state AFM clock model [(0.13–0.25) [38] and (0.1–0.275) [45]], and TAFI model with 2NN ferromagnetic interactions (0.15–0.27) [47].

The calculation of the Binder magnetic fourth-order cumulant U_B^m also demonstrated that transitions at T_1 and T_2 belong to a universality class of the BKT-type phase transitions. The $U_B^m(L)$ vs $U_B^m(L')$ plots revealed that basically $U_B^m(L) \to U_B^m(L')$ with increase of $L' < L$, and, consequently,

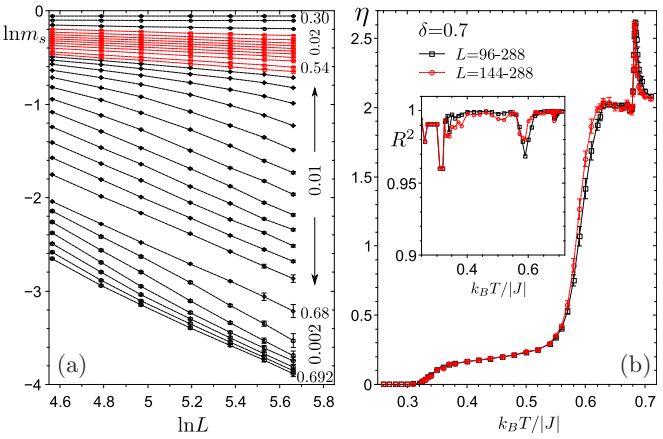

FIG. 4. (Color online) (a) Log-log plot of m_s vs L for 3NN12 model at $\delta = 0.7$ in a temperature interval comprising the phase transition points at T_1, T_2, and T_c. The BKT-type transition region is shown by red lines. (b) Temperature dependence of parameter η calculated for seven (black curve) and five largest (red curve) lattice sizes. Inset: Temperature dependence of a linear fit accuracy parameter R^2 for both cases.

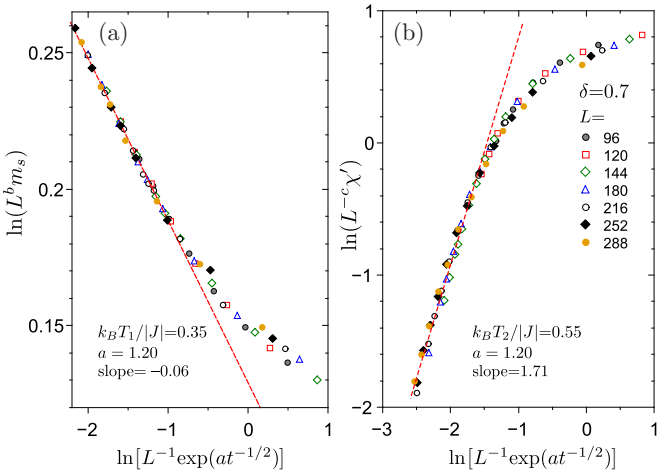

FIG. 5. (Color online) Finite-size scaling of (a) m_s at T_1 [$t = (T_1 - T)/T_1$] and (b) χ' at T_2 [$t = (T - T_2)/T_2$] for the 3NN12 model at $\delta = 0.7$ obtained using first and second scaling relations (4), respectively.

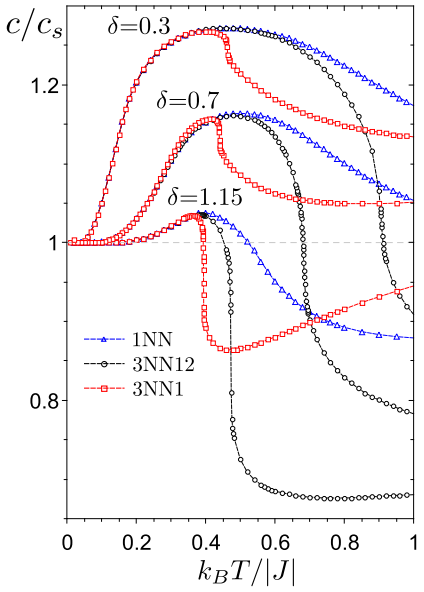

FIG. 6. (Color online) Temperature dependence of concentration for three models at $L = 120$: 1NN (blue triangles), 3NN12 (black squares), and 3NN1 (red squares) at $\delta = 0.3$, 0.7, and 1.15.

$\nu \to \infty$ in the formula, $\partial U_B^m(L')/\partial U_B^m(L) = (L'/L)^{1/\nu}$, as for the BKT-type phase transition point.

The $\eta(T)$ dependence [Fig. 4(b)] is also sensitive to the point at T_c demonstrating a sharp peak at the same value of temperature where the extrema of D_{1s}, D_{2s}, and C_v are obtained. This is not unexpected: the T_c is the phase transition point. The high value of η at T_c makes it impossible to assign this transition to a universality class of the BKT-type transitions. If the phase transition would be of the second order, the order parameter at T_c should scale as $\sim L^{-\beta/\nu}$. However, the value of β/ν is much too large and inconsistent with the second-order phase transition. This is the indication that the first-order phase transition might take place at T_c.

We noticed that this transition occurs at approximately the same concentration of particles as the stoichiometric concentration of the low-temperature LRO AFM phase (see Fig. 6). Visual inspection of instant particle configuration reveals a marked increase (in comparison to the paramagnetic phase) of hexagons with side length $2a$ and alternation of $+1$ and -1 variables on the vertices and 0 in the center, i.e., hexagons typical to the low-T phase of the 3NN12 model. These domains of low-temperature phase exist in a very small interval of temperature between T_c and T_2. Decrease of temperature from T_c leads to an increase of concentration, which results in a population of centers of mentioned hexagons and the formation of a frustrated structure at T_2, the structure which further continues up to the phase transition point at T_1. This increase of concentration is rather abrupt in comparison to a smooth and continuous increase of c characteristic to the 1NN model (cf. the curves in Fig. 6). Thus, at T_c, we obtain a strongly diluted phase with domains of the low-temperature AFM LRO phase. It is known that dilution in frustrated systems leads to phase transitions with nonclassical critical exponents, broad two-maxima histograms with high saddle point, ambiguous behavior of interface energy, and, in general, makes the FSS analysis very complicated [48].

The energy histograms at T_c and $\delta = 0.7$ are shown in Fig. 7. They are two peaked and remain such up to the largest lattice size studied here, $L = 399$. Using these histograms, we calculated interface tension, $2\sigma = \ln[P_{\max}(L)/P_{\min}(L)]/L$, and latent heat, $\Delta E = |E_+ - E_-|$. Here, $P_{\max}(L)$ and $P_{\min}(L)$ are the probability density of energy at the maximum and saddle point, respectively; $E_+(L)$ and $E_-(L)$ are the energies at the right and left peaks of energy distribution, respectively. The 2σ even up to $L = 399$ (limit of our computer resources) depends on L—thus, we are not sure if we have reached the lattice sizes suitable for the finite-size scaling. The saddle point slightly decreases with L, which would indicate in favor of the first-order phase transition, though the behavior is rather different from that of the typical first-order phase transition. The interface tension and latent heat decrease with an increase of L, as shown in Figs. 7(b) and 7(c). The ΔE, most likely, tends to a finite value.

The results of the FSS analysis of specific heat close to T_c are given in Fig. 8(a). We obtain the following values of critical exponent ratios: $\alpha/\nu = 1.04 \pm 0.05$ and $1/\nu = 1.64 \pm 0.05$ at $\delta = 0.7$. The calculation of α/ν from the magnitude of C_v peak at T_c yields the same result [see Fig. 8(c)]. The calculation of $1/\nu$ from the minima of D_{1s} and D_{2s} at T_c gives us a much smaller critical exponent of the correlation length, $1/\nu = 1.0 \pm 0.05$.

We also performed histograms and critical exponents calculation at another point of region I, $\delta = 0.3$. The saddle point of these histograms is even higher than that at $\delta = 0.7$, and correspondingly the interface tension is a bit smaller. The latent heat is similar to that of $\delta = 0.7$. The scaling performed at $\delta = 0.3$ yields the following critical exponents: $\alpha/\nu = 0.83 \pm 0.05$ and $1/\nu = 1.5 \pm 0.05$. The critical exponent obtained by scaling the parameters D_{1s} and D_{2s} at T_c is $1/\nu = 1.0 \pm 0.05$, i.e., the same as for $\delta = 0.7$.

Thus, in range I at T_c, we do not obtain standard values of critical exponents. The behavior of thermodynamic parameters at T_c is much smoother than that in ranges II and III, where the first-order phase transition is found (Secs. III B and III C). Therefore, we assume either a weak first-order phase transition, as often encountered in models with site or bond dilution [48], or a second-order phase transition with the latent heat approaching zero at such values of L which exceed our computer resources. We do not exclude the possibility that the critical exponents might slightly change for a considerable increase of L.

It should be noted though that at $\delta = 0.7$, the obtained set of critical exponents is rather close to the one obtained by Landau [47] for the tricritical region of the TAFI model with ferromagnetic 2NN interactions ($\alpha/\nu = 1.02$ and $1/\nu = 1.59$).

B. 3NN12 model at other values of δ (ranges II and III)

The transition in range III ($1.3 < \delta < 1.5$ and $T_c = T_2 = T_1$) is clearly of the first order. It is demonstrated by energy histograms for $\delta = 1.3$ and 1.45 presented in Fig. 9. The saddle point in this region is much lower than in range I and it decreases with an increase of L.

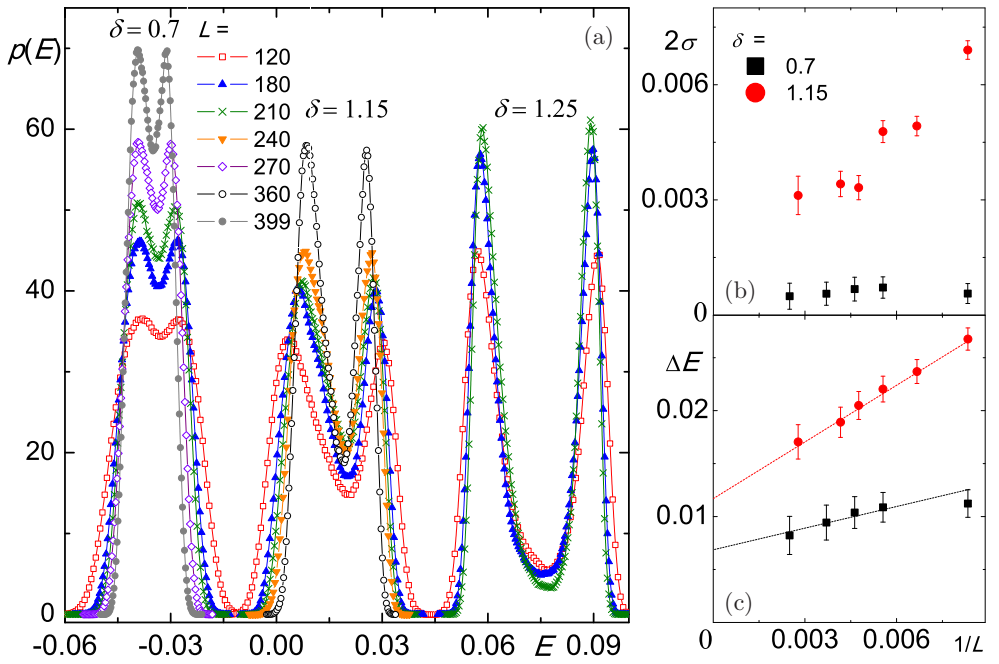

FIG. 7. (Color online) (a) Energy histograms of the 3NN12 model at $\delta = 0.7$, 1.15, and 1.25 (the latter is shifted along the energy axis by 0.05). The L dependence of (b) interface tension and (c) latent heat.

The same, just not as strong, tendency to the first-order phase transitions is seen in range II ($1.15 < \delta < 1.3$ and $T_c \approx T_2 > T_1$). We have chosen the points $\delta = 1.15$ and $\delta = 1.25$ for a more thorough examination (see histograms in Fig. 7). The interface tension and latent heat are much higher at these points than in range I. With respect to transition order at T_c, this range is intermediate between the ambivalent-order phase transition in range I and the first-order phase transition in range III.

Different properties of the phase transition at T_c in ranges II and III, on one hand, and range I, on the other hand, might be seen by analyzing the δ dependence of energy histograms at fixed L [Fig. 9(a)], in particular—interface tension [Fig. 9(b)] and latent heat [Fig. 9(c)]. It is seen that both

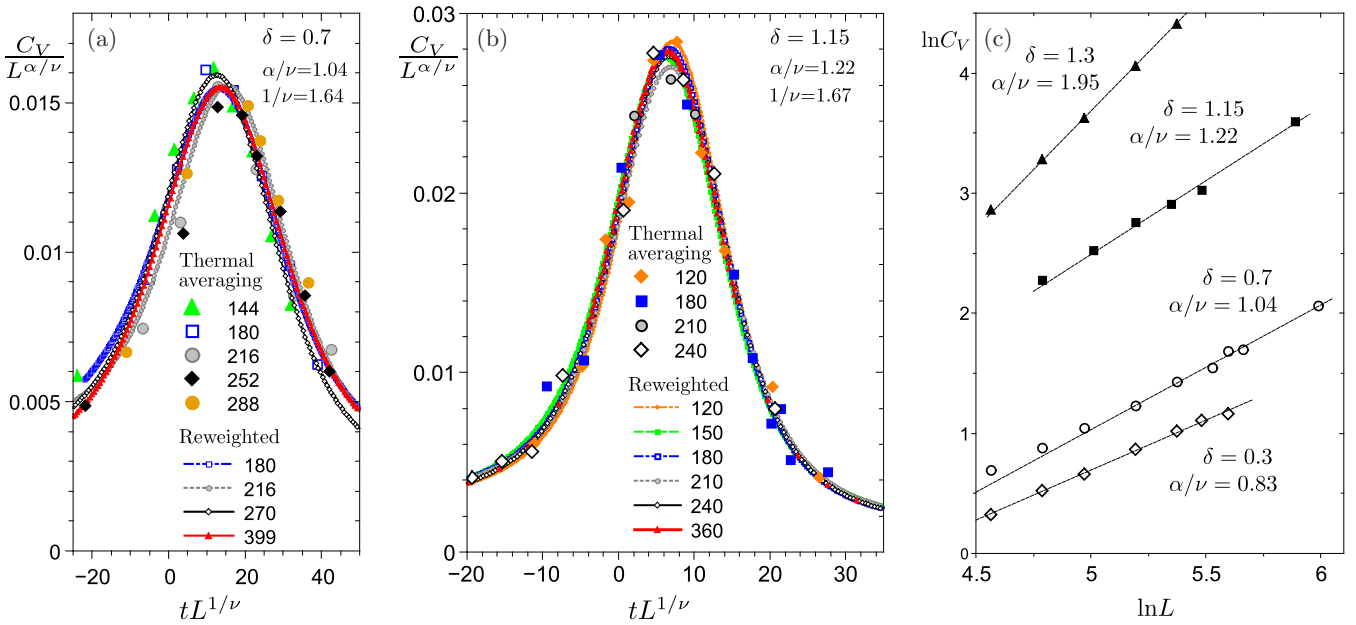

FIG. 8. (Color online) Finite-size scaling of specific heat of the 3NN12 model: (a) $\delta = 0.7$ and (b) 1.15. The results are fitted using formula $C_v - C_0 \sim L^{\alpha/\nu} f(tL^{1/\nu})$, where $t = |T_c - T|/T_c$ and the background is assumed to be $C_0 = 0$. Large symbols correspond to the results of thermal averaging; lines and small symbols correspond to results obtained close to T_c by the reweighted histogram method. (c) Log-log dependences of C_v maximum vs L at different values of δ.

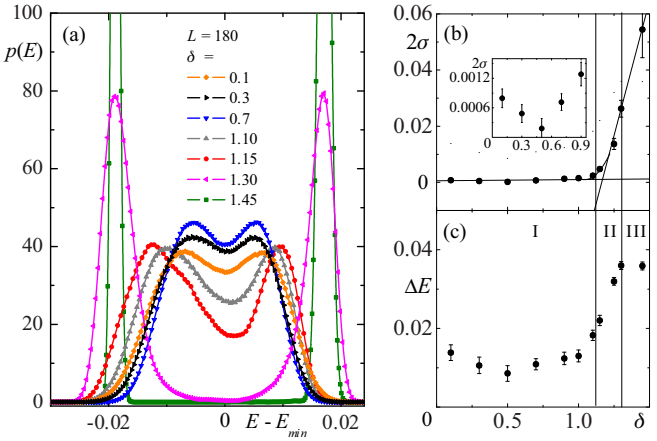

FIG. 9. (Color online) (a) Energy histograms at various values of δ at T_c for $L = 180$ lattice. Corresponding δ dependences of (b) interface tension (zoomed-in version in inset) and (c) latent heat.

these parameters increase for higher values of δ. Here we can notice the separation of the system into three mentioned ranges of behavior: range I featuring two-peaked histograms with high saddle point, range III demonstrating typical first-order phase transition, and the intermediate range II. In Fig. 9(b), the intersection of two lines corresponding to types of behavior in ranges I and III is around 1.1–1.2 for $L = 180$. It should be noted that the behavior at $0 < \delta < 0.9$ is not as homogeneous as might be assumed from the main part of Fig. 9(b). The detailed inset in Fig. 9(b) demonstrates that interface tension slightly increases when the limit of the TAFI model, $\delta = 0$, is approached, and therefore has some minimum around $\delta \approx 0.5$. This minimum also survives in calculations with other lattice sizes.

A rather similar result is obtained analyzing the magnitude of the minimum related to T_c of both Binder cumulants, $U_B^m(T_c)$ and $U_B^E(T_c)$. They have two very different regions of behavior: up to approximately $\delta = 0.9$, the minimum of U_B^m is around 0.3–0.1, but drastically decreases for higher values of δ. The minimum of U_B^E is rather close to the 2/3 limit up to $\delta = 0.7$, but again starts to rather abruptly decrease at higher values of δ.

The results of our thermal averaging MC simulation in ranges II and III demonstrate that the thermodynamic parameters close to T_c either show thin and high extrema (C_v and D_{1s}, D_{2s}) or abruptness similar to jump (m_s and average energy); see, e.g., the behavior of normalized coverage at $\delta = 1.15$ in Fig. 6. These results confirm the results obtained by histogram calculations that the phase transitions in these two regions are of the first order.

In ranges II and III, we also performed FSS analysis and determined the ratios of critical exponents. We obtained $\alpha/\nu =$ 1.22, 1.68, and 1.95 (± 0.05) and $1/\nu = 1.67$, 1.94, and 1.99 (± 0.05) for $\delta = 1.15$, 1.25, and 1.3, respectively. Some results of this analysis are presented in Figs. 8(b) and 8(c). While the values of α/ν and $1/\nu$ at limiting points of the range II, $\delta = 1.25$ and 1.3, tend to the value 2 and are further stabilized at $d = 2$ for $\delta > 1.3$ (range III), the values at the other limiting point, $\delta = 1.15$, are closer to those of the range I (and the point $\delta = 0.7$, in particular).

Thus, if the transitions in range I turned out to be of the second order, then range II would be the tricritical region. It is interesting that the theoretical prediction for the tricritical point of the three-state Potts model ($\alpha/\nu = 10/7 = 1.43$ and $1/\nu = 12/7 = 1.71$ [49]) is in between our values at $\delta = 1.15$ and 1.25.

C. 3NN1 model (ranges II and III)

The exclusion of interactions on 1NN distances leaves more sites for the diffusion of particles in the 3NN1 model in comparison to the 1NN and 3NN12 models. Higher entropy than in these models leads to a decrease of the phase transition temperature from the paramagnetic phase T_c: it occurs in the limits of the critical line of the BKT-type phase transition points. Therefore, the T_c in region II ($0 < \delta \lesssim 1.2$) becomes hardly separable from the high-temperature end of this line, T_2. Thus, the question arises if the point at $T_2 \approx T_c$ is the higher-temperature end of the BKT-type phase transitions, as in the 1NN model, or has the properties of the first-order phase transition, as in the region II of the 3NN12 model.

The $m_s(T)$ dependence at $\delta = 0.7$ is given in Fig. 10(a). There is no qualitative change in comparison to the 1NN and 3NN12 models at T_1, where we observe the low-temperature BKT-type phase transition. At $T_2 \approx T_c$, the $m_s(T)$ curve is weakly dependent on L, which would make it a likely candidate for the BKT-type transition. On the other hand, the dependence at this point is very abrupt, as in the case of the first-order phase transition. The peak of susceptibility [inset in Fig. 10(a)] at $T_2 \approx T_c$ is much higher than that of the 3NN12 model at $T_2 < T_c$, but comparable with the one obtained in the 3NN12 model when $T_2 \approx T_c$ at $1.15 < \delta <$ 1.3. The specific heat demonstrates a sharp L-dependent peak at $T_2 \approx T_c$ [Figs. 10(b) and 10(c)] which clearly increases with increase of δ [Fig. 10(e)]. The peak of C_v at T_1 is almost L independent. It is also very small in comparison with the main peak [Fig. 10(d)].

The log-log plots of m_s vs T dependence [Fig. 11(a)] and, consequently, η vs T dependence in Fig. 11(b) clearly demonstrate the region of the BKT-type phase transitions and T_1 as its low-temperature end ($\eta \sim 0.12$ at T_1). However, the high-temperature end of the BKT-type transitions line shows a high peak at $T_c \approx T_2$ instead of rounding which is characteristic to T_2 encountered in the 1NN and 3NN12 models. Moreover, the FSS analysis of the phase transition point close to T_1 might be performed [see Fig. 12(a)] using the first formula (4), and the best fit gives $T_1 = 0.34 \pm$ 0.01 and $\eta(T_1) = 0.12 \pm 0.02$. However, the FSS analysis using the second formula (4) close to $T_c \approx T_2$ is rather unsuccessful.

The critical behavior at the $T_2 \approx T_c$ peak of $\eta(T)$ dependence is also inconsistent with any reasonable β/ν values related to the second-order phase transition. All of these facts indicate that for the 3NN1 model, the transition at T_1 is the BKT-type phase transition, but the high-temperature transition at $T_c \approx T_2$ is not. The latter conclusion is further confirmed by the histograms calculation. The saddle point in the two-peak energy histograms of Fig. 13(a) at $\delta = 0.7$ rather

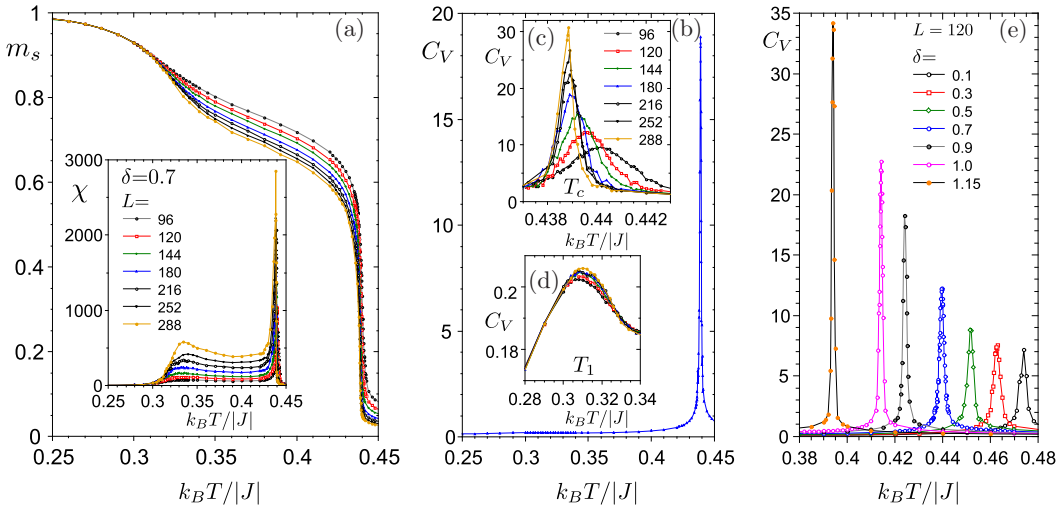

FIG. 10. (Color online) Temperature dependence of (a) staggered magnetization, (inset a) susceptibility, and (c), (d) specific heat close to transition points $T_2 \approx T_c$ and T_1 of the 3NN1 model at $\delta = 0.7$ and different values of L. (b) The $C_v(T)$ dependence at $\delta = 0.7$ and $L = 120$. (e) The $C_v(T)$ dependence at $L = 120$ and different values of δ.

systematically decreases with increase of L, supporting the idea of the first-order phase transition at this point.

One more argument in favor of the first-order phase transition at $T_c \approx T_2$ of the 3NN1 model in region II comes from analysis of the autocorrelation time of energy. As mentioned, the integrated autocorrelation time for the 3NN1 model at $\delta = 0.7$ and $T_c \approx T_2$ is around one to two orders of magnitude higher than for the 3NN12 model at $\delta = 0.7$ and $T_c > T_2$, and is approximately $\tau \sim 10^4$–10^5 for $L = 120$ and close to the limit of our calculations, $\tau \sim 10^6$–10^7, for $L = 399$. Such difference between the autocorrelation times for both models indicates the much stronger first-order nature of the 3NN1 model transition.

Nevertheless, the extrema of the C_v, D_{1s}, and D_{2s} parameters in region II at $T_c \approx T_2$ do not scale with L^2 as for the usual first-order phase transition. This is clearly seen extending the lattice sizes up to $L = 399$. The C_v scales with critical exponents $\alpha/\nu = 0.97 \pm 0.05$ and $1/\nu = 1.55 \pm 0.05$ [Fig. 12(b)]. The FSS of the D_{1s} and D_{2s} parameters gives a very similar result for $1/\nu$. The same is true when $1/\nu$ is obtained from scaling of $T_c(L) = T_c(\infty) + aL^{-1/\nu}$, when $T_c(\infty)$ is the one used for scaling in Fig. 12(b).

Thus, our results in range II imply that the two transitions at T_2 and T_c are separate transitions at two very close temperature points (as in some other frustrated systems [37,50]). This is seen from the FSS results in Fig. 11 for the 3NN1 model

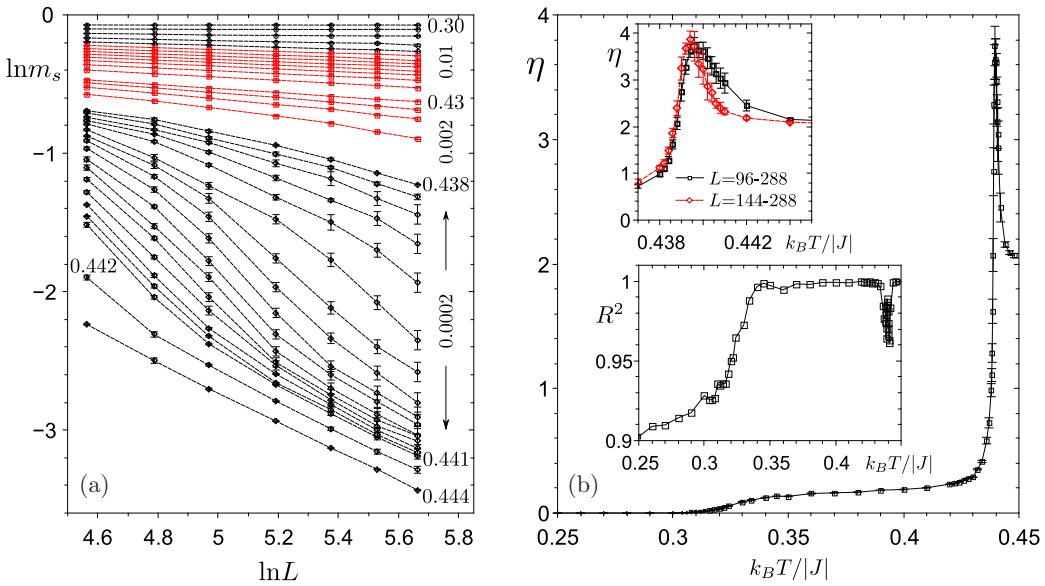

FIG. 11. (Color online) (a) Log-log plot of m_s vs L for the 3NN1 model at $\delta = 0.7$ in a temperature interval comprising the phase transition points at T_1, T_2, and T_c. The BKT-type transition region is shown by red lines. (b) Temperature dependence of parameter η obtained from (a). Insets: (upper) $\eta(T)$ dependence close to T_c peak for the five (black curve) and three largest (red curve) lattice sizes, respectively; (lower) temperature dependence of a linear fit accuracy parameter R^2.

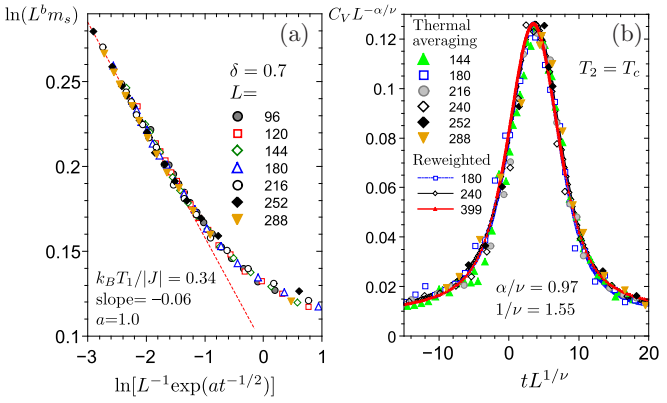

FIG. 12. (Color online) Finite-size scaling of the 3NN1 model parameters at $\delta = 0.7$: (a) m_s at T_1 [$t = (T_1 - T)/T_1$] and (b) C_v at $T_c \approx T_2$ using scaling relation $C_v \sim L^{\alpha/\nu} f(tL^{1/\nu})$, where $t = |T_c - T|/T_c$.

and very similar results for the 3NN12 model at $\delta = 1.15$. The parameter η in Fig. 11 is around 0.3 (higher limit of the BKT-type phase) up to T_2 and then jumps abruptly to the maximum value with slight increase of temperature. The maximum of η is obviously related to the phase transition at T_c, which is shown to be of the first order by the histograms calculation. On the other hand, the critical line of the BKT-type points has to have its highest temperature point at T_2 until the BKT-type phase exists. Certainly, these two phase transition points are extremely close and their proximity further increases excluding small lattices from consideration [see inset in Fig. 11(b)]. Thus, though we notice some tendency of these points to merge with further increase of lattice size L, within the accuracy of our calculations, they should be separate transitions with $T_c \gtrsim T_2$.

The first-order type of transition at $\delta > 1.2$ (region III) is much more explicit than at $\delta = 0.7$. The critical exponents tend to the value 2, demonstrating typical first-order behavior. The extrema of C_v, D_{1s}, and D_{2s} clearly scale as $\sim L^2$ even when smaller lattices are used for the analysis.

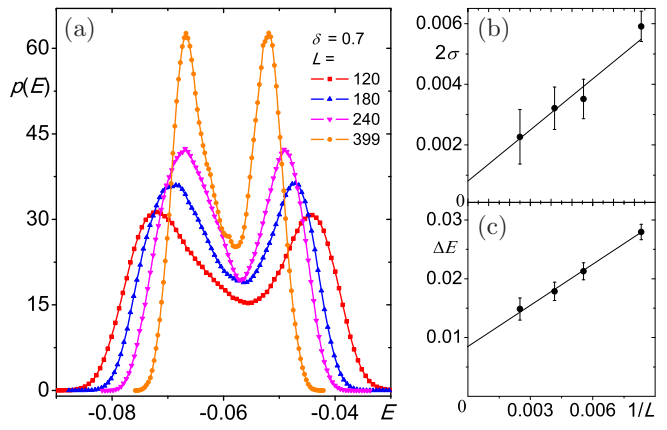

FIG. 13. (Color online) (a) Energy histograms, (b) interface tension $2\sigma = \frac{1}{L}\ln(P_{\max}/P_{\min})$, and (c) latent heat of the 3NN1 model at $\delta = 0.7$.

IV. DISCUSSION

Both 3NN models with exclusions, as well as the 1NN model, possess the BKT-type frustrated structure in between the temperature points T_1 and T_2. The temperature range between these two points decreases with an increase of a single-ion anisotropy parameter δ, until the two BKT-type transitions flow into one first-order phase transition from the paramagnetic to the AFM LRO phase at δ_c. The $\delta_c = 1.47$ [39], 1.3, and 1.2 for the 1NN, 3NN12, and 3NN1 models, respectively. Phase diagrams of all three models are presented in Figs. 14(a), 14(b), and 14(d). It is seen that in the range $0 < \delta < \delta_c$, the low-temperature phase transition temperature T_1 does not depend on the model.

The value δ_c, characterizing the limit of the BKT-type phase ($T_1 = T_2$), was obtained studying the extrema of temperature dependences of functions C_v, χ, U_B^m, D_{1s}, and D_{2s} for different values of δ. The spread of T_1 values (as well as T_2 values) among all these different functions was rather small. It is known, however, that the values of T_1 and T_2 obtained from these extrema slightly differ from those obtained using the FSS analysis (4). The results of the FSS analysis for the 3NN12 model are presented in Fig. 14(b) by gray dots. Though the mismatch of results given by these two methods decreases with an increase of δ, the value of δ_c obtained using FSS (4) is 1.3 (to compare with $\delta_c \approx 1.35$ obtained from the extrema of mentioned functions).

Let us compare the high-temperature phase transitions of 1NN and 3NN12 models in more detail. The 1NN model demonstrates the paramagnetic-to-BKT-type phase transition at T_2. The 3NN12 model shows two transitions: from the paramagnetic phase to the structure, which has the stoichiometry and separate domains of the LRO AFM phase at T_c, and the higher-temperature transition to the BKT-type phase at T_2. The frustrated phase in the 3NN12 model disorders at lower temperature than in the 1NN model because the 3NN12 model has higher entropy, i.e., a larger number of free sites for hopping and higher probability of inhomogeneous distribution of particles into domains.

The occurrence of the phase transition at T_c is related to the fact that exclusions create an inhomogeneous distribution of particles in the disordered phase and, as a result, make the energy and other thermodynamic functions more abrupt at higher temperature. Thus, an income of particles is hindered and their coverage c is artificially maintained too small for that particular temperature (in comparison to the 1NN model). A decrease of temperature enhances AFM correlations and the "normal" coverage is recovered by a sudden increase of c. This might be seen, e.g., in the $c(T)$ dependences in Fig. 6, where the hump in the $c(T)$ dependence marks the region of frustrated phase, or the temperature dependences of internal energy, which cause sharp peaks of C_v at T_c. The "semiordered" AFM phase has a chance to form in the 3NN12 model, since the favorable conditions (relatively low temperature and stoichiometry of the AFM phase) allow for the AFM domains phase to occur just before the hump. Higher concentration and correspondingly broader hump (lower values of δ) shift the T_c value to higher temperature, while lower concentration ($\delta > 1$) makes the hump small and $T_c \to T_2$ (Fig. 6).

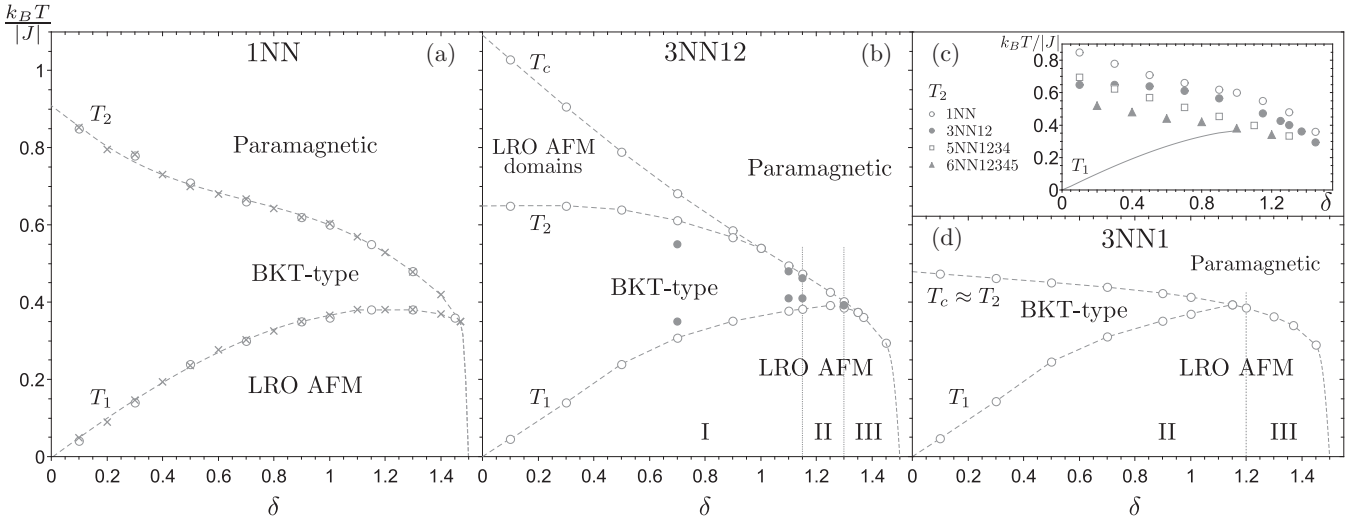

FIG. 14. The phase diagrams of all three models: (a) 1NN ($L = 48$), (b) 3NN12 ($L = 180$), and (d) 3NN1 ($L = 180$). (c) The dependence of transition temperature $T_c \approx T_2$ on a chosen model with full exclusion (see text). The crosses in (a) are the results of Ref. [39]. The gray dots in (b) are the results of the FSS calculations using formula (4). Dashed lines are guides to the eye.

The entropy of the 3NN1 model is even higher than that of the 1NN or 3NN12 models and therefore the temperature of the phase transition from the paramagnetic phase is the lowest of all three models. Moreover, this phase transition in the 3NN1 model occurs at such a value of temperature that lies within temperature limits of the BKT-type phase in the 1NN model. Therefore, contrary to the 1NN model, which has the line of critical BKT-type points between T_1 and T_2, and the 3NN12 model, which (at least in a part of δ range) demonstrates three phase transitions (T_1, T_2, and T_c), the 3NN1 model shows a reduced temperature interval of the BKT-type phase. The end point of this phase at T_2 almost coincides with T_c for all values of δ. An analogous situation is in the 3NN12 model at a narrow range, $1.15 < \delta < 1.3$. As shown in Sec. III C, we obtain two separate transitions at very close temperature points ($T_c \gtrsim T_2$). Note, however, that here we did not study the nature of the planar phase. Therefore, we did not introduce the order parameter for the BKT-type phase transition. By employing two order parameters, it might be possible to study both of these transitions separately, in order to determine if they merge or not [as for, e.g., the six-state clock [37,38] and fully frustrated XY (FFXY) [50] models].

It should be noted that the 3NN12 model is a unique model in which the distinction of higher-temperature phase transitions at T_c and T_2 is clearly seen. In addition to this model, two other models with full exclusions up to the interaction distance were also studied: the 5NN model with exclusions up to 4NN (5NN1234) and the 6NN model with exclusions up to 5NN (6NN12345). Within the accuracy of our calculations, all models except 3NN12 demonstrate two transitions at one temperature point at $T_c \approx T_2$. The transition temperature at this point and the parameter δ_c in all models with full exclusions for entropic reasons gradually decreases with increase of interaction distance of the model [see Fig. 14(c)].

The obtained energy histograms at T_c of both 3NN12 and 3NN1 models were found to be two peaked in a whole range of δ values. However, the height of the saddle point in these histograms clearly depends on δ. The δ dependences of interface tension, latent heat, and Binder cumulants demonstrate that there are three ranges of behavior of phase transitions. In range III, the transition at $T_c = T_2 = T_1$ is clearly of the first order. This is evidenced by two-peaked histograms with a saddle point which is either very deep or decreasing with an increase of L. The magnitudes of critical exponents α/ν and $1/\nu$ are close to 2. The histograms in intermediate range II (at $T_c \approx T_2 > T_1$) have a higher saddle point than those in region III, but they also decrease with an increase of L. This allows one to attribute the transition at T_c in this range to the first order as well. However, in this range, the finite-size scaling at the T_c point gives critical exponents different from (though rather close to) 2.

We could not give a definite answer on the type of phase transition at T_c in range I of the 3NN12 model. The obtained energy histograms are two peaked, but the saddle point is rather high. Extrapolation of the values of interface tension and latent heat at lattice sizes used in this paper shows that they approach finite limits at $L \to \infty$. The thermodynamic functions at the phase transition are rather smooth in this range and the obtained critical exponents are nonstandard. This would allow one to attribute the transition to "weak" first-order phase transitions observed in some diluted and frustrated systems [48]. Nevertheless, we cannot completely rule out the possibility of a classical phase transition. An analysis of scaling corrections to specific heat at T_c in range I demonstrates that either very large lattice sizes are needed to obtain the critical exponent of the first-order phase transition or the critical exponents are nonstandard.

A similar phase diagram as of the 3NN12 model might be observed in other frustrated systems. The phase transitions from the paramagnetic to fully frustrated phase in the square ϕ^4 FFXY model [50] proceed either through (i) an Ising and BKT phase transitions sequence with very close transition temperatures (at small values of parameter D similar to our δ), (ii) a tricritical region (intermediate values of D) featuring

histograms with high saddle point, or (iii) first-order phase transitions (high values of D).

Here we studied strongly diluted lattices with small concentration of particles (spins). Such studies require huge computer resources and therefore might leave some questions not completely answered. However, the main tendencies are quite clear: exclusions do not affect the low-temperature phase transition; they make the high-temperature phase transition more abrupt; rescaling of the lattice stimulates the entropic effects and decreases the high-temperature phase transition temperature; in a case of the 3NN12 model, the formation of domains of low-temperature structure might reveal itself as a phase transition at high temperature.

ACKNOWLEDGMENTS

We are grateful to Wolfhard Janke for reading the manuscript and valuable discussions. A.I. acknowledges funding support by the European Union Structural Funds project, Postdoctoral Fellowship Implementation in Lithuania (Grant No. VP1-3.1-MM-01-V-02-004).

[1] L. Bartels, Nat. Chem. **2**, 87 (2010).
[2] J. V. Barth, Annu. Rev. Phys. Chem. **58**, 375 (2007).
[3] A. Dmitriev, N. Lin, J. Weckesser, J. V. Barth, and K. Kern, J. Phys. Chem. B **106**, 6907 (2002).
[4] Z. Li, B. Han, L. J. Wan, and Th. Wandlowski, Langmuir **21**, 6915 (2005).
[5] Y. C. Ye, W. Sun, Y. F. Wang, X. Shao, X. G. Xu, F. Cheng, J. L. Li, and K. Wu, J. Phys. Chem. C **111**, 10138 (2007).
[6] S. Griessl, M. Lackinger, M. Edelwirth, M. Hietschold, and W. M. Heckl, Single Mol. **3**, 25 (2002).
[7] M. Lackinger, S. Griessl, W. M. Heckl, M. Hietschold, and G. W. Flynn, Langmuir **21**, 4984 (2005).
[8] K. G. Nath, O. Ivasenko, J. M. MacLeod, J. A. Miwa, J. D. Wuest, A. Nanci, D. F. Perepichka, and F. Rosei, J. Phys. Chem. C **111**, 16996 (2007).
[9] L. Kampschulte, T. L. Werblowsky, R. S. K. Kishore, M. Schmittel, W. M. Heckl, and M. Lackinger, J. Am. Chem. Soc. **130**, 8502 (2008).
[10] R. Gutzler, T. Sirtl, J. F. Dienstmaier, K. Mahata, V. M. Heckl, M. Schmittel, and M. Lackinger, J. Am. Chem. Soc. **132**, 5084 (2010).
[11] J. A. Theobald, N. S. Oxtoby, M. A. Phillips, N. R. Champness, and P. H. Beton, Nature (London) **424**, 1029 (2003).
[12] U. K. Weber, V. M. Burlakov, L. M. A. Perdigao, R. H. J. Fawcett, P. H. Beton, N. R. Champness, J. H. Jefferson, G. A. D. Briggs, and D. G. Pettifor, Phys. Rev. Lett. **100**, 156101 (2008).
[13] F. Silly, U. K. Weber, A. Q. Shaw, V. M. Burlakov, M. R. Castell, G. A. D. Briggs, and D. G. Pettifor, Phys. Rev. B **77**, 201408 (2008).
[14] Y. Li, Z. Ma, G. Qi, Y. Yang, Q. Zeng, X. Fan, C. Wang, and W. Huang, J. Phys. Chem. C **112**, 8649 (2008).
[15] A. Ciesielski, P. J. Szabelski, W. Rzysko, A. Cadeddu, T. R. Cook, P. J. Stang, and P. Samori, J. Am. Chem. Soc. **135**, 6942 (2013).
[16] G. Pawin, K. L. Wong, K.-Y. Kwon, and L. Bartels, Science **313**, 961 (2006).
[17] T. Misiūnas and E. E. Tornau, J. Phys. Chem. B **116**, 2472 (2012).
[18] G. M. Bell and D. A. Lavis, J. Phys. A: Gen. Phys. **3**, 568 (1970).
[19] C. E. Fiore, M. M. Szortyka, M. C. Barbosa, and V. B. Henriques, J. Chem. Phys. **131**, 164506 (2009).
[20] M. Blume, Phys. Rev. **141**, 517 (1966); H. W. Capel, Physica (Utrecht) **32**, 966 (1966).
[21] A. N. Berker and M. Wortis, Phys. Rev. B **14**, 4946 (1976); G. D. Mahan and S. M. Girvin, *ibid.* **17**, 4411 (1978); J. Adler, A. Aharony, and J. Oitmaa, J. Phys. A: Math. Gen. **11**, 963 (1978).
[22] M. Kaufman, R. B. Griffiths, J. M. Yeomans, and M. E. Fisher, Phys. Rev. B **23**, 3448 (1981).
[23] J. B. Collins, P. A. Rikvold, and E. T. Gawlinski, Phys. Rev. B **38**, 6741 (1988).
[24] M. Blume, V. J. Emery, and R. B. Griffiths, Phys. Rev. A **4**, 1071 (1971); J. Sivardiere and J. Lajzerowicz, *ibid.* **11**, 2090 (1975).
[25] A. P. Young and D. A. Lavis, J. Phys. A: Gen. Phys. **12**, 229 (1979).
[26] M. A. A. Barbosa and V. B. Henriques, Phys. Rev. E **77**, 051204 (2008).
[27] R. M. F. Houtappel, Physica (Utrecht) **16**, 425 (1950); G. H. Wannier, Phys. Rev. **79**, 357 (1950); R. J. Baxter, J. Phys. A **13**, L61 (1980).
[28] A. Ibenskas and E. E. Tornau, Phys. Rev. E **86**, 051118 (2012).
[29] V. Petrauskas, S. Lapinskas, and E. E. Tornau, J. Chem. Phys. **120**, 11815 (2004).
[30] S. Fortuna, D. L. Cheung, and A. Troisi, J. Phys. Chem. B **114**, 1849 (2010).
[31] M. Šimėnas, A. Ibenskas, and E. E. Tornau, Phase Trans. **86**, 866 (2013).
[32] M. Šimėnas and E. E. Tornau, J. Chem. Phys. **139**, 154711 (2013).
[33] M. Schick, J. S. Walker, and M. Wortis, Phys. Rev. B **16**, 2205 (1977); A. N. Berker, S. Ostlund, and F. A. Putnam, *ibid.* **17**, 3650 (1978).
[34] W. F. Wreszinski and S. R. A. Salinas, *Disorder and Competition in Soluble Lattice Models*, Series on Advances in Statistical Mechanics (World Scientific, Singapore, 1993), Vol. 9.
[35] S. Miyashita, Proc. Jpn. Acad. Ser. B **86**, 643 (2010); S. Miyashita, H. Kitatani, and Y. Kanada, J. Phys. Soc. Jpn. **60**, 1523 (1991).
[36] J. L. Cardy, J. Phys. A: Math. Gen. **13**, 1507 (1980).
[37] J. D. Noh, H. Rieger, M. Enderle, and K. Knorr, Phys. Rev. E **66**, 026111 (2002).
[38] T. Surungan, Y. Okabe, and Y. Tomita, J. Phys. A: Math. Gen. **37**, 4219 (2004).
[39] M. Žukovič and A. Bobák, Phys. Rev. E **87**, 032121 (2013).
[40] P. D. Coddington and L. Han, Phys. Rev. B **50**, 3058 (1994).
[41] A. M. Ferrenberg and R. H. Swendsen, Phys. Rev. Lett. **61**, 2635 (1988); **63**, 1658 (1989).

[42] A. M. Ferrenberg and D. P. Landau, Phys. Rev. B **44**, 5081 (1991).
[43] M. S. S. Challa, D. P. Landau, and K. Binder, Phys. Rev. B **34**, 1841 (1986).
[44] J. M. Kosterlitz and D. J. Thouless, J. Phys. C: Solid State Phys. **6**, 1181 (1973).
[45] M. S. S. Challa and D. P. Landau, Phys. Rev. B **33**, 437 (1986).
[46] J. V. José, L. P. Kadanoff, S. Kirkpatrick, and D. R. Nelson, Phys. Rev. B **16**, 1217 (1977).
[47] D. P. Landau, Phys. Rev. B **27**, 5604 (1983).
[48] C. Chatelain, P.-E. Berche, B. Berche, and W. Janke, Comp. Phys. Comm. **147**, 431 (2002); S. Jin, A. Sen, W. Guo, and A. W. Sandvik, Phys. Rev. B **87**, 144406 (2013); A. Kalz and A. Honecker, *ibid.* **86**, 134410 (2012).
[49] M. P. M. den Nijs, J. Phys. A **12**, 1857 (1979); B. Nienhuis, A. N. Berker, E. K. Riedel, and M. Schick, Phys. Rev. Lett. **43**, 737 (1979); B. Nienhuis, J. Phys. A **15**, 199 (1982).
[50] M. Hasenbusch, A. Pelissetto, and E. Vicari, J. Stat. Mech. (2005) P12002; Phys. Rev. B **72**, 184502 (2005).